Charge-Driven Selective Adsorption of Sodium Dodecyl Sulfate on Graphene Oxide Visualized by Atomic Force Microscopy

ARTICLE *in* THE JOURNAL OF PHYSICAL CHEMISTRY C · SEPTEMBER 2012

Impact Factor: 4.77 · DOI: 10.1021/jp305717v

3 AUTHORS, INCLUDING:

Douglas H. Adamson
University of Connecticut
114 PUBLICATIONS **8,744** CITATIONS

SEE PROFILE

Hannes Schniepp
College of William and Mary
34 PUBLICATIONS **7,166** CITATIONS

SEE PROFILE

THE JOURNAL OF PHYSICAL CHEMISTRY C

Article

pubs.acs.org/JPCC

Charge-Driven Selective Adsorption of Sodium Dodecyl Sulfate on Graphene Oxide Visualized by Atomic Force Microscopy

A. Jaeton Glover,[†] Douglas H. Adamson,[‡] and Hannes C. Schniepp*,[†]

[†]Department of Applied Science, The College of William & Mary, Williamsburg, Virginia 23185, United States

[‡]Institute of Materials Science Polymer Program, University of Connecticut, Storrs, Connecticut 06269, United States

Supporting Information

ABSTRACT: Using liquid-cell atomic force microscopy, we investigated molecular adsorption of sodium dodecyl sulfate (SDS) from aqueous solution onto single-layer graphenes that were oxidized to different degrees. SDS did not adsorb onto graphene oxide (GO) featuring an atomic carbon:oxygen (C:O) ratio of 2.0. Reduced GO (C:O ratio: 10.7), in contrast, was covered with micellar SDS aggregates, featuring a height of ≈2 nm and lateral feature sizes of ≈5 nm. This selective adsorption depending on the degree of oxidation can be explained by electrostatic repulsion between the negatively charged SDS head groups and the negatively charged hydroxyl groups on oxidized graphene. Our results suggest it will be possible to translate this adsorption selectivity into separation techniques that fractionate GO into subsets featuring different degrees of oxidation. Such fractionation techniques are likely to enable the preparation of GO with more well-defined electronic properties and make GO interesting as a band gap material.

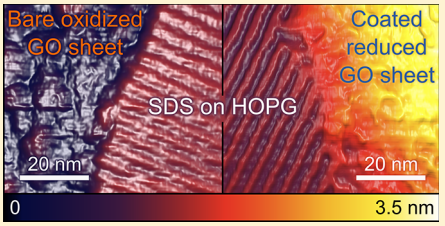

INTRODUCTION

Graphene, the single-layer, two-dimensional form of graphite, shows great potential as an electronic and optoelectronic material.[1−6] However, as it is a semimetal with a zero band gap in its native state, its use is impeded in applications requiring finite size band gaps.[1−7] Therefore, several methods have been utilized to introduce a band gap to graphene, including the application of uniaxial strain,[8−13] dimensional control in quantum-confined nanoribbons,[14−19] or selection of multilayer graphenes with specific thicknesses.[20] However, for each of these approaches, significant technical challenges need to be overcome; scalable preparation of graphene with a band gap based on these techniques has not yet been demonstrated. A potentially useful method is the attachment of oxygen-containing functional groups to disrupt graphene's π-bond character, thereby creating a band gap.[21−26] This is readily achieved through a chemical oxidation reaction carried out on bulk graphite and can thus easily be translated to a large scale economically. What currently hinders the viability of this method is that the reaction is difficult to control, rendering the resulting material, graphene oxide (GO), strongly heterogeneous: GO has band gaps ranging from 0.25 to 2.4 eV and can hence be considered highly impure with respect to its optoelectronic properties.[22−26] Subsequent attempts to create a material with more well-defined band gaps via chemical or thermal treatments after the oxidation have remained unsatisfying.[21−29]

Our goal is to address this problem by separating as-produced GO into fractions with narrowly defined band gaps. Hersam et al. have described the separation of multilayer graphene according to the number of layers of which they are comprised via centrifugation with the aid of the surfactant sodium cholate.[20] In similar work, the selective adsorption of surfactants on to single-walled carbon nanotubes (SWNTs) according to physical characteristics such as chirality and diameter has been reported.[30−38] Subsequent density gradient centrifugation separation schemes have yielded SWNTs with varying band gaps.[30−34] Thus, a strategy to fractionate GO according to band gaps becomes feasible once molecules are identified that exhibit selective adsorption on GO depending on electronic properties. This approach would enable large-scale, low-cost production of materials with well-defined, selectable band gaps.

Photoluminescence experiments have shown that the band gap in GO arises upon oxidation, where hydroxyl and epoxy groups are attached to the graphitic backbone,[21,39] thereby converting many carbon atoms from sp^2 to sp^3 hybridization. The emergence of the band gap has been explained by a quantum-containment effect, where oxidized sites create nodes in wave functions of delocalized electrons and are defined by the spacing of the oxide groups.[21] The oxidation is typically carried out through the Hummers reaction, which uses strong acids and oxidizers.[40−44] The reported issues with reproducibility and heterogeneity[22−26,45−48] of the obtained GO materials can be attributed to inefficient mixing and heat transfer as the viscosity of the reaction mixture increases.

Our strategy to achieve selective adsorption is to employ charged molecules, since GO assumes a negative surface charge in aqueous environment due to proton dissociation from the hydroxyl groups.[49,50] Consequently, the GO regions that are

Received: June 12, 2012
Revised: August 17, 2012
Published: August 25, 2012

more oxidized will feature a higher density of negative surface charges and are also expected to have larger band gaps. Conversely, less oxidized regions are expected to feature smaller band gaps and a lower density of negative surface charges. Hence, positively charged molecules are expected to have a greater affinity for GO sheets with larger band gaps, whereas molecules with negative charge are expected to be repelled from such areas. Here we present our investigation of this phenomenon using the anionic surfactant sodium dodecyl sulfate (SDS).

The often utilized and well-understood surfactant SDS[51] has good solubility in water and is known to adsorb from aqueous solution onto many surfaces, including graphite[52−55] and gold[56−58] at concentrations of a few weight percent. SDS forms wormlike aggregates on graphite and gold surfaces, which are a few nanometers in height and diameter; they are generally believed to be of hemicylindrical morphology.[53−55,57,58] Such surfactant surface aggregates can be visualized at the solid−solution interface using liquid-cell atomic force microscopy (AFM).[53−55,57−60] Surfactant aggregation is governed by a delicate balance of several forces, including van der Waals attraction, electrostatic repulsion, and hydrophobic interactions. On solid surfaces, surfactant aggregation is thus affected by subtle changes in the substrate properties such as topography[58,61] or crystal structure.[59−64] It is thus feasible that SDS adsorption is modulated by the surface charge density of GO. Using liquid-cell AFM, we are able to directly visualize how SDS behaves on GO that is oxidized to different degrees. This approach enables us to evaluate SDS for the desired, band-gap-selective adsorption behavior on oxidized graphene at the level of individual sheets and with spatial resolutions of a few nanometers.

MATERIALS AND METHODS

Synthesis and Characterization of GO and Reduced GO Samples. Graphite oxide was produced from flake graphite (Grade 3243, Asbury Carbons, Asbury, NJ) using the Hummers method.[42] Portions of the product were then thermally reduced and exfoliated via rapid heating[65,66] in a crucible in 100 mg batches. To determine the elemental compositions of as-produced GO and thermally reduced GO (rGO), samples of these materials were first dried at a temperature <50 °C under vacuum (pressure <30 hPa) for 4.5 h and then tested via elemental analysis (Galbraith Laboratories, Inc., Knoxville, TN). The C:O ratios for the GO and rGO were determined to be 2.1 and 10.7, respectively, which is in good agreement with the literature.[65−69]

Preparation of AFM Samples. Dry samples with single-layer GO and rGO on freshly cleaved ZYH-grade highly oriented pyrolytic graphite (HOPG) substrates (NT-MDT, Zelenograd, Moscow, Russia) were prepared first. GO was acoustically exfoliated and dispersed into ultrapure water with a measured resistance of 18.2 MΩ (Millipore Synergy water system, Millipore, Billerica, MA) using a 100 W Microson XL2007 tip sonicator (Microson, Farmingdale, NY) at 0.1 mg/mL for 1 h.[67−69] The resulting, stable GO suspension, which had no visible unexfoliated particles, was further diluted with ultrapure water to 0.01 mg/mL and spin-coated at 2000 rpm for 3 min onto HOPG. AFM investigation of these samples showed that practically all GO was completely exfoliated into single layers (see Supporting Information). For the reduced material, rGO, dimethylformamide (DMF, anhydrous, 99.8%, Sigma-Aldrich, St. Louis, MO) was chosen as a solvent, due to the increased hydrophobicity of rGO. Dispersion was carried out using ultrasonication, as above, at an original concentration of 0.1 mg/mL and then diluted to 0.01 mg/mL. This suspension was also stable and free of undispersed material. It was spin-coated onto HOPG in the same manner as GO.

Liquid-Cell AFM in SDS Solutions. The dry GO and rGO samples were then exposed to aqueous SDS solutions and imaged using liquid-cell AFM. Solutions were made using SDS (99%, Aldrich) and ultrapure water. To minimize hydrolysis of SDS,[53] solutions were used within 24 h of preparation. Images were taken with a MultiMode AFM (Bruker, Santa Barbara, CA) coupled with a NanoScope IIId controller using a liquid cell (model designator MTFML). The liquid cell was assembled and used after flushing with ≈5 mL of surfactant solution (≈10 times the volume of the cell). CSG01 silicon AFM probes without reflective coating were used (NT-MDT, Zelenograd, Russia). The probes have a tip radius of curvature <10 nm and a spring constant of 0.03 N/m (nominal values). After assembly, the liquid-cell AFM was allowed to equilibrate for a minimum of 1 h to reduce drifts. All imaging was carried out in static mode at constant cantilever deflection, at different force set points. Surfactant surface aggregates were imaged in "precontact mode"[54,59−63] with low set points, optimized for best micellar contrast. Higher set force points were used to image the substrate below the adsorbed molecules.[54] Typical scanning speeds were 3 μm/s; integral and proportional gains were increased to highest stable values (typical "I-Gain" and "P-Gain" settings in the Bruker Nanoscope control software were around 5). All AFM data shown is topography data; images were treated using first-order polynomial line-by-line leveling[70] to compensate for vertical drifts, as is typical in AFM. Images were then processed using spatial median and spatial low-pass filters to remove noise.

RESULTS AND DISCUSSION

We first imaged GO sheets on HOPG using liquid-cell AFM in ultrapure water (without SDS). The topography data of this control experiment is presented in Figure 1a, showing that all visible GO sheets are single layer with lateral sheet sizes of several hundreds of nanometers and sheet heights of about 0.8 nm, in agreement with the literature.[27,67−69] The GO sheets

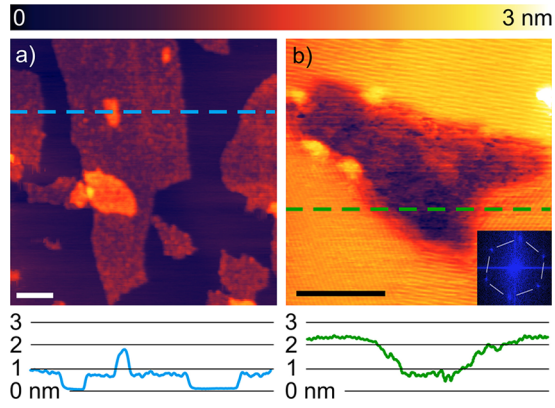

Figure 1. (a) GO on HOPG in pure water (AFM topography). (b) The same sample imaged in 10 mM SDS. The dark GO sheet in the center is lower than the surrounding areas representing HOPG covered by a 2 nm thick layer of SDS. (b, inset) FFT of the image. Topography sections along the dashed blue and green lines in (a) and (b) are shown at the bottom. Scale bars = 100 nm.

dx.doi.org/10.1021/jp305717v | J. Phys. Chem. C 2012, 116, 20080−20085

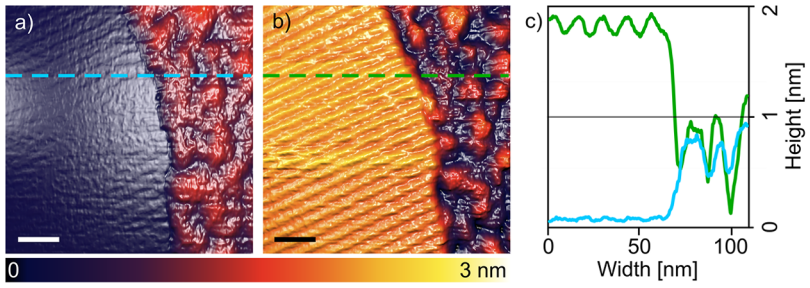

Figure 2. (a) High-force scan showing the sample below the SDS layer; accordingly, GO (right) is higher than the HOPG substrate (left). Scale bar = 20 nm. (b) Low-force scan revealing a 2 nm high SDS population on HOPG (left) but not on GO (right), which remains unchanged. Scale bar = 20 nm. (c) Overlay of cross sections from (a) and (b) showing that the SDS layer on HOPG is higher than the uncovered GO.

feature the typical intrinsic roughness in comparison to the completely flat HOPG substrate.[59] This is further supported by the topography cross section following the blue dashed line in Figure 1a shown in the bottom of the figure.

In the second experiment, a 10 mM SDS solution was used, a concentration significantly higher than the threshold above which micellar SDS adsorption is known to occur on HOPG (2−3 mM).[53] Liquid-cell AFM was carried out using a very low force set point (precontact mode, topography data shown in Figure 1b) in order to reveal any micellar surfactant aggregates adsorbed on the sample surface. In comparison to the image taken without surfactants (Figure 1a), Figure 1b exhibits contrast inversion: the GO sheets (such as the one in the center of Figure 1b) appear darker than the areas around them, which means that they are lower. This is also evident in the topography section following the green dashed line in Figure 1b, which is displayed in the bottom of the figure. This finding can be explained as follows. As expected for a 10 mM SDS concentration, a layer of surfactants, on the order of 2 nm thick,[53] adsorbs on the HOPG substrate and thus increases its measured height. The fact that the 1 nm thick GO sheets appear lower than the surrounding substrate areas, coated in a 2 nm thick surfactant layer, suggests that SDS does not adsorb on the GO sheets.

Closer inspection of Figure 1b reveals the structure of the layer of micellar surfactant aggregates on HOPG. The corresponding brighter areas in Figure 1b feature a pattern of equidistant, parallel lines with a spacing of 5.3 ± 0.5 nm. This is in excellent agreement with literature reports of SDS surface aggregates on HOPG: they are close-packed, straight hemicylinders featuring periodicities of about 5 nm.[54] Moreover, the Fourier transform of Figure 1b, featured as an inset, shows that the hemicylinder orientations in the different patches in Figure 1b exhibit relative angles of 120°. This symmetry confirms that the hemicylinders are oriented perpendicular to the ⟨1000⟩ directions on the graphite surface, as expected.[54,71]

One further experiment was carried out to test our hypothesis that in a 10 mM SDS solution there are no micelles on GO, while HOPG is covered by surfactant surface aggregates. Parts a and b of Figure 2 feature liquid-cell AFM scans of exactly the same sample region taken at two different force set points. Figure 2a was carried out with a vertical force several hundred piconewtons higher than in Figure 1. Under these conditions, the AFM probe pushes through the layer of adsorbed surfactants and makes direct contact with the surface below the surfactants.[54,60,61] Accordingly, the left, darker side of the image shows the HOPG substrate, while the right side shows the beginning of a GO sheet with its characteristic rough surface. The cross section plotted as a blue line in Figure 2c shows topography data along the blue dashed line in Figure 2a. The data in Figure 2a and the corresponding cross section in Figure 2c are in excellent agreement with the data shown in Figure 1a, which confirms that the high-force image essentially represents the sample topography without surfactants.

The same sample region is then imaged using a low-force set point, so that the AFM probe is stable in the precontact regime, which allows imaging the surfactant population on the sample (see Figure 2b).[61] The right side of this image looks very similar to Figure 2a; most features of the GO sheet can be identified in parts a and b of Figure 2, which proves that exactly the same sample area is imaged. The left-hand side of Figure 2b, in contrast, looks very different than Figure 2a. Under low-force imaging conditions, the parallel and straight hemicylindrical SDS surface micelles on HOPG are clearly revealed. The corresponding topography cross section in Figure 2c shows that the added height due to the adsorbed surfactant layer on the left side of Figure 2b is about 2 nm and shows periodic oscillations representing the morphology of equidistant hemicylinders, as expected. Surfactants are found on HOPG but not on GO, and the adsorbed surfactant layer (≈2 nm) is thicker (higher) than the GO sheets (≈1 nm), which leads to the discussed contrast inversion in Figure 1. Depending on whether the sample is imaged without (high force) or with surfactants (low force), the GO sheets appear as positive or negative topography features.

A more detailed look at the AFM data in Figure 2 reveals a few additional aspects. First, the topography of the GO sheets exhibits a systematic difference between the high- and the low-force images shown in panels a and b. The height variations in the high-force image, representing the typical intrinsic "wrinkling" of GO sheets, are less pronounced compared to the low-force image. This can also be seen by comparing the differences in modulation heights between the blue and the green curves on the right-hand side of Figure 2c. A possible explanation is that there is a small gap between the sheets and the substrate below the wrinkles and that these areas are then temporarily compressed as the AFM probe moves across them at higher vertical force. Second, the left-hand side of Figure 2a shows a few faint periodic ripples where the low-force image (Figure 2b) shows the hemicylindrical micelles. This seems surprising, since Figure 2a was taken at a force set point high enough that the AFM tip pushes through the surfactant layer and establishes contact with the substrate. However, it is known that a lateral force is induced as the tip moves through the micelles.[54] The ripples shown in Figure 2a are thus likely due to cross-talk causing this lateral force to induce a pseudodeflection signal, which the control loop translates into subangstrom topography and which becomes visible due to very low levels of

dx.doi.org/10.1021/jp305717v | J. Phys. Chem. C 2012, 116, 20080−20085

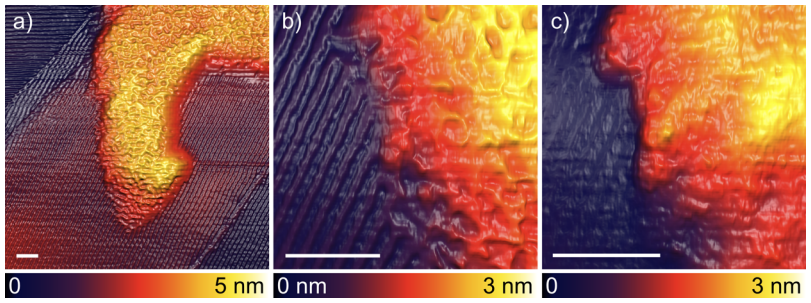

Figure 3. (a, b) Low-force AFM images revealing SDS on both rGO and HOPG at different magnifications. (c) High-force image of the same region as in (b) showing the sample without SDS. Scale bars = 25 nm.

noise present in our data. As a third point, we note that some of the horizontal scan lines below the middle of Figure 2b appear brighter than the lines above and below (especially toward the right-hand side of the figure, where micelles are shown). This apparent height difference is not actual topography; instead, it is due to thermal drifts of the instrument, for which our leveling algorithm was unable to compensate.

The main conclusions from Figures 1 and 2 are that we observe SDS adsorption on HOPG, whereas there is no micellar adsorption of SDS on GO at the same SDS concentration of 10 mM. It is known that in aqueous solution, SDS is only weakly bound on HOPG via hydrophobic interactions (physisorption).[72] GO, in contrast, is known to feature negative surface charges,[49,50] which repel the negatively charged SDS molecules and thus hinder SDS adsorption. Since HOPG is chemically identical to pristine graphene, this evidence suggests that we identified a surfactant system that selectively adsorbs on zero-band-gap pristine graphene, but not to oxidized graphene, which has a finite band gap. These data are a proof-of-principle demonstration that techniques to separate GO from pristine graphene can be developed using SDS surfactant. However, our ultimate goal goes further: to fractionate all sheets within a batch of GO into fractions with band gaps as narrowly defined as possible. For this goal a stronger degree of selectivity is needed. We need to distinguish not only between graphene sheets that are oxidized or pristine but also between sheets featuring different degrees of oxidation. To investigate this selectivity, the experiments were repeated with the reduced GO (rGO) sheets featuring a C:O ratio of 10.7.

Liquid-cell AFM images of rGO on HOPG exposed to a 10 mM aqueous SDS solution were taken at low and high forces, and the results are shown in Figure 3. As we will show, these reduced GO sheets are completely covered with surfactant micelles, in stark contrast to what we observed on regular GO sheets. Figure 3a was taken at low force to reveal the surfactant population on the sample. The darker areas show well-aligned and straight micelle hemicylinders suggesting they are located on top of HOPG. This is further supported by the fact that these areas are flat and that micelles are only oriented in two different directions with a relative angle of 120°. One can also see three diagonal topography steps that are typical for ledges on HOPG surfaces. The bright area in the center of the image represents an rGO sheet; the fact that it is higher than the surrounding micelles on HOPG suggests the rGO sheet is also covered in SDS. Interestingly, the adsorbed surfactant layer features totally different structures on rGO in comparison to HOPG. While the surfactants form relatively long, straight hemicylinders on HOPG, the aggregates exhibit a "spongy" morphology on rGO. This structure is featured at higher magnification in Figure 3b.

Finally, Figure 3c shows a high-force image of exactly the same sample area. As expected, the HOPG substrate appears almost perfectly flat under high-force conditions. The rGO sheet does not change its general shape; only the spongy surface texture, now proven to be due to the surfactant, vanishes. Figure 3c thus provides the final confirmation for our interpretation of parts a and b of Figure 3. Parts b and c of Figure 3 use exactly the same vertical scale (0−3 nm), and the rGO sheet has the same average color in both images; the same is true for the HOPG background. This means that the relative heights remain constant at high and low forces—with or without surfactants. Thus, we can conclude that the adsorbed surfactant layer has approximately the same thickness on both materials. This can be rationalized by the fact that most of the oxygen-containing functional groups have been removed in rGO, which makes it chemically similar to HOPG.

The higher-magnification image in Figure 4 shows that the adsorbed surfactant layer on rGO features holes with an average

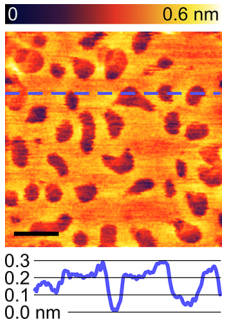

Figure 4. High-magnification scan of SDS adsorbed onto rGO surface. Holes in the surfactant layer are ≈4 nm across and 0.14 nm in depth. Scale bar = 10 nm.

diameter of ≈4 nm. The apparent depth of the holes is only a fraction of 1 nm. However, this is likely a significant underestimate due to the finite size of the AFM probe; we suspect the holes reach all the way to the rGO sheet. This measurement of the detailed morphology of the adsorbed SDS layer allowed us to estimate the total amount of surfactant attached to each sheet, in order to assess the effectiveness of subsequent mass-based separation methods. Using image analysis we determined that the surfactant covers approximately 77 ± 2% of the rGO sheet (see Supporting Information for details). We estimated the mass of the adsorbed surfactant layer and found that an SDS-coated rGO sheet would be about five times as massive as an uncoated sheet.[51,73−75] This is a

dx.doi.org/10.1021/jp305717v | J. Phys. Chem. C 2012, 116, 20080−20085

substantial increase, promising good separation sensitivity. For pristine graphene (infinite C:O ratio), we assume complete coverage, like on HOPG, which leads to a sixfold relative mass increase (see Supporting Information on these estimates). A possible explanation for the existence of these holes is that they occur at sites where the density of hydroxyl groups on the rGO sheets is higher than average. Due to the negative charge of these groups, micellar adsorption would be inhibited in these areas, whereas the density of functional groups in the remaining 77% is low enough to allow adsorption. At this point this is a hypothesis that needs further testing. If confirmed, liquid-cell AFM of surfactant-covered functionalized graphene would provide a powerful tool to reveal the surface chemistry of these sheets with sub-5 nm resolution. For more highly oxidized sheets featuring a lower C:O ratio, we expect larger holes and less sheet coverage. According to this rationale, the mass gain of oxidized graphene is a monotonically increasing function of the C:O ratio.

CONCLUSIONS

We visualized micellar surfactant adsorption on graphenes for the first time. We demonstrated that SDS adsorption onto functionalized graphene sheets strongly depends on the degree of graphene oxidation. This makes band-gap-selective molecular adsorption on graphene feasible, which has great potential for application in separation with the goal of enriching GO sheets with particular electronic properties. The examples investigated here demonstrate a strong discrimination between GO with a C:O ratio of 2 on one hand, where no SDS adsorption is observed, and rGO sheets (C:O ratio 10.7) on the other hand, which are fully covered with SDS micelles at an SDS concentration of 10 mM. Further experiments will have to show at which C:O ratio the transition between the two scenarios occurs and how sharp this transition is. We hypothesize that this transition can be controlled by adjusting solution parameters such as the pH or the ionic strength via addition of various salts.[30,76−81] Increasing the ionic strength reduces the range of the electrostatic forces in the solution and is thus expected to effectively diminish the electrostatically driven inhibition of SDS adsorption on GO sheets. Consequently, we suppose that the threshold C:O ratio above which SDS adsorption takes place is lowered if the ionic strength is increased. Lowering the pH decreases the surface charge of GO sheets and is thus expected to have a similar effect. Further fine-tuning of surfactant behavior may be achieved by using surfactants with different counterions.[82] We thus envision that molecular adsorption approaches will provide the basis for fine-grained separation processes that enable the separation of oxidized graphenes into fractions with well-defined electronic band gaps. Ultimately, this work aims at transforming GO into a high-quality optoelectronic material.

ASSOCIATED CONTENT

Supporting Information

Additional GO characterization, detailed calculations for determination of surfactant coverage of rGO, and detailed calculations for sheet mass estimates. This material is available free of charge via the Internet at http://pubs.acs.org.

AUTHOR INFORMATION

Corresponding Author

*E-mail schniepp@wm.edu, phone +1-757-221-2559, fax +1-757-221-2050.

Notes

The authors declare no competing financial interest.

ACKNOWLEDGMENTS

This material is based upon work supported by the National Science Foundation under Grant Nos. DMR-1111021 and DMR-1111030.

REFERENCES

(1) Geim, A. K.; Novoselov, K. S. *Nat. Mater.* **2007**, *6*, 183−191.
(2) Bonaccorso, F.; Sun, Z.; Hasan, T.; Ferrari, A. C. *Nat. Photonics* **2010**, *4*, 611−622.
(3) Zhu, Y.; Murali, S.; Cai, W.; Li, X.; Suk, J. W.; Potts, J. R.; Ruoff, R. S. *Adv. Mater.* **2010**, *22*, 3906−3924.
(4) Zhang, Y.; Tan, Y.-W.; Stormer, H. L.; Kim, P. *Nature* **2005**, *438*, 201−204.
(5) Novoselov, K. S.; Geim, A. K.; Morozov, S. V.; Jiang, D.; Zhang, Y.; Dubonos, S. V.; Grigorieva, I. V.; Firsov, A. A. *Science* **2004**, *306*, 666−669.
(6) Novoselov, K. S.; Jiang, D.; Schedin, F.; Booth, T. J.; Khotkevich, V. V.; Morozov, S. V.; Geim, A. K. *Proc. Natl. Acad. Sci. U.S.A.* **2005**, *102*, 10451−10453.
(7) Yong, V.; Tour, J. M. *Small* **2009**, *6*, 313−318.
(8) Gui, G.; Li., J.; Zhong, J. *Phys. Rev. B* **2008**, *78*, 075435.
(9) Guinea, F.; Katsnelson, M. I.; Geim, A. K. *Nat. Phys.* **2010**, *6*, 30−33.
(10) Ni, Z. H.; Yu, T.; Lu, Y. H.; Wang, Y. Y.; Feng, Y. P.; Shen, Z. X. *ACS Nano* **2008**, *2*, 2301−2305.
(11) Pereira, V. M.; Neto, A. H. C.; Peres, N. M. R. *Phys. Rev. B* **2009**, *80*, 045401.
(12) Yang, L.; Anantram, M. P.; Han, J.; Lu, J. P. *Phys. Rev. B* **1999**, *60*, 13874−13878.
(13) Yu, T.; Ni, Z.; Du, C.; You, Y.; Wang, Y.; Shen, Z. *J. Phys. Chem. C* **2008**, *112*, 12602−12605.
(14) Barone, V.; Hod, O.; Scuseria, G. E. *Nano Lett.* **2006**, *6*, 2748−2754.
(15) Son, Y.; Cohen, M. L.; Louie, S. G. *Nature* **2006**, *444*, 347−349.
(16) Brey, L.; Fertig, H. A. *Phys. Rev. B.* **2006**, *73*, 235411.
(17) Li, X.; Wang, X.; Zhang, L.; Lee, S.; Dai, H. *Science* **2008**, *319*, 1229−1232.
(18) Kusakabe, K.; Maruyama, M. *Phys. Rev. B.* **2003**, *67*, 092406.
(19) Han, M. Y.; Özyilmaz, B.; Zhang, Y.; Kim, P. *Phys. Rev. Lett.* **2007**, *98*, 206805.
(20) Green, A. A.; Hersam, M. C. *Nano Lett.* **2009**, *9*, 4031−4036.
(21) Luo, Z.; Vora, P.; Mele, E.; Johnson, A. T. C.; Kikkawa, J. M. *Appl. Phys. Lett.* **2009**, *94*, 111909.
(22) Boukhvalov, D. W.; Katsnelson, M. I. *J. Am. Chem. Soc.* **2008**, *130*, 10697−10701.
(23) Jeong, H. K.; Jin, M. H.; So, K. P.; Lim, S. C.; Lee, Y. H. *J. Phys. D: Appl. Phys.* **2009**, *42*, 065418.
(24) Lahaye, R. J. W. E.; Jeong, H. K.; Park, C. Y.; Lee, Y. H. *Phys. Rev. B* **2009**, *79*, 125435.
(25) Yan, J.-A.; Xian, L.; Chou, M. Y. *Phys. Rev. Lett.* **2009**, *103*, 086802.
(26) Jin, M.; Jeong, H.-K.; Yu, W. J.; Bae, D. J.; Kang, B. R.; Lee, Y. H. *J. Phys. D: Appl. Phys.* **2009**, *42*, 135109.
(27) Glover, A. J.; Cai, M.; Overdeep, K. R.; Kranbuehl, D. E.; Schniepp, H. C. *Macromolecules* **2011**, *44*, 9821−9829.
(28) Shen, Y.; Zhou, P.; Sun, Q. Q.; Wan, L.; Li, J.; Chen, L. Y.; Zhang, D. W.; Wang, X. B. *Appl. Phys. Lett.* **2011**, *99*, 141911.
(29) Wei, Z.; Wang, D.; Kim, S.; Kim, S.-Y.; Hu, Y.; Yakes, M. K.; Laracuente, A. R.; Dai, Z.; Marder, S. R.; Berger, C.; King, W. P.; de Heer, W. A.; Sheehan, P. E.; Riedo, E. *Science* **2010**, *328*, 1373−1376.
(30) Niyogi, S.; Densmore, C. G.; Doorn, S. K. *J. Am. Chem. Soc.* **2009**, *131*, 1144−1153.
(31) Arnold, M. S.; Suntivich, J.; Stupp, S. I.; Hersam, M. C. *ACS Nano* **2008**, *2*, 2291−2300.

(32) Arnold, M. S.; Stupp, S. I.; Hersam, M. C. *Nano Lett.* **2005**, *5*, 713−718.
(33) Arnold, M. S.; Green, A. A.; Hulvat, J. F.; Stupp, S. I.; Hersam, M. C. *Nat. Nanotechnol.* **2006**, *1*, 60−65.
(34) Ju, S.-Y.; Doll, J.; Sharma, I.; Papadimitrakopoulos, F. *Nat. Nanotechnol.* **2008**, *3*, 356−362.
(35) Richard, C.; Balavoine, F.; Schultz, P.; Ebbesen, T. W.; Mioskowski, C. *Science* **2003**, *300*, 775−778.
(36) McDonald, T. J.; Engtrakul, C.; Jones, M.; Rumbles, G.; Heben, M. J. *J. Phys. Chem. B* **2006**, *110*, 25339−25346.
(37) Tummala, N. R.; Striolo, A. *Phys. Rev. E* **2009**, *80*, 021408.
(38) Tummala, N. R.; Morrow, B. H.; Resasco, D. E.; Striolo, A. *ACS Nano* **2010**, *4*, 7193−7204.
(39) Kudin, K. N.; Ozbas, B.; Schniepp, H. C.; Prud'homme, R. K.; Aksay, I. A.; Car, R. *Nano Lett.* **2008**, *8*, 36−41.
(40) Cai, W.; Piner, R. D.; Stadermann, F. J.; Park, S.; Shaibat, M. A.; Ishii, Y.; Yang, D.; Velamakanni, A.; An, S. J.; Stoller, M.; An, J.; Chen, D.; Ruoff, R. S. *Science* **2008**, *321*, 1815−1817.
(41) Szabó, T.; Berkesi, O.; Forgó, P; Josepovits, K.; Sanakis, Y.; Petridis, D.; Dékány, I. *Chem. Mater.* **2006**, *18*, 2740−2749.
(42) Hummers, W. S., Jr.; Offeman, R. E. *J. Am. Chem. Soc.* **1958**, *80*, 1339.
(43) Mkhoyan, K. A.; Contryman, A. W.; Silcox, J.; Stewart, D. A.; Eda, G.; Mattevi, C.; Miller, S.; Chhowalla, M. *Nano Lett.* **2009**, *9*, 1058−1063.
(44) Lerf, A.; He, H.; Forster, M.; Klinowski, J. *J. Phys. Chem. B* **1998**, *102*, 4477−4482.
(45) Eda, G.; Chhowalla, M. *Adv. Mater.* **2010**, *22*, 2392−2415.
(46) Gomez-Navarro, C.; Weitz, R. T.; Bittner, A. M.; Scolari, M.; Mews, A.; Burghard, M.; Kern, K. *Nano Lett.* **2007**, *7*, 3499−3503.
(47) Erickson, K.; Erni, R.; Lee, Z.; Alem, N.; Gannett, W.; Zettl, A. *Adv. Mater.* **2010**, *22*, 4467−4472.
(48) Schniepp, H. C.; Kudin, K. N.; Li, J.-L.; Prud'homme, R. K.; Car, R.; Saville, D. A.; Aksay, I. A. *ACS Nano* **2008**, *2*, 2577−2584.
(49) Szabó, T.; Tombácz, E.; Illés, E.; Dékány, I. *Carbon* **2006**, *44*, 537−545.
(50) Li, D.; Müller, M. B.; Gilje, S.; Kaner, R. B.; Wallace, G. G. *Nat. Nanotechnol.* **2008**, *3*, 101−105.
(51) Manda, A.; Nair, B.; Ramaswamy, D. *Langmuir* **1988**, *4*, 736−739.
(52) Hey, M. J.; Mactaggart, J. W.; Rochester, C. H. *J. Chem. Soc., Faraday Trans. 1* **1984**, *80*, 699−707.
(53) Wanless, E. J.; Ducker, W. A. *J. Phys. Chem.* **1996**, *100*, 3207−3214.
(54) Schniepp, H. C.; Saville, D. A.; Aksay, I. A. *J. Am. Chem. Soc.* **2006**, *128*, 12378−12379.
(55) Tummala, N. R.; Grady, B. P.; Striolo, A. *Phys. Chem. Chem. Phys.* **2010**, *12*, 13137−13143.
(56) Brenton, D. P.; Sparks, B. D. *Trans. Faraday Soc.* **1967**, *63*, 3244−3252.
(57) Burgess, I.; Jeffrey, C. A.; Cai, X.; Szymanski, G.; Galus, Z.; Lipkowski, J. *Langmuir* **1999**, *15*, 2607.
(58) Schniepp, H. C.; Shum, H. C.; Saville, D. A.; Aksay, I. A. *J. Phys. Chem. B* **2006**, *111*, 8708.
(59) Manne, S.; Cleveland, J. P.; Gaub, H. E.; Stucky, G. D.; Hansma, P. K. *Langmuir* **1994**, *10*, 4409.
(60) Manne, S.; Gaub, H. E. *Science* **1995**, *270*, 1480−1482.
(61) Schniepp, H. C.; Shum, H. C.; Saville, D. A.; Aksay, I. A. *J. Phys. Chem. C* **2008**, *112*, 14902−14906.
(62) Schniepp, H. C.; Saville, D. A.; Aksay, I. A. *Langmuir* **2008**, *24*, 626−631.
(63) Saville, D. A.; Chun, J.; Li, J.-L.; Schniepp, H. C.; Car, R.; Aksay, I. A. *Phys. Rev. Lett.* **2006**, *96*, 018301.
(64) Li, J.-L.; Schniepp, H. C.; Aksay, I. A.; Car, R. *Nano LIFE* **2012**, *02*, 1240001.
(65) Schniepp, H. C.; Li, J.-L.; McAllister, M. J.; Sai, H.; Herrera-Alonso, M.; Adamson, D. H.; Prud'homme, R. K.; Car, R.; Saville, D. A.; Aksay, I. A. *J. Phys. Chem. B* **2006**, *110*, 8535−8539.
(66) McAllister, M. J.; Li, J.-L.; Adamson, D. H.; Schniepp, H. C.; Abdala, A. A.; Liu, J.; Herrera-Alonso, M.; Milius, D. L.; Car, R.; Prud'homme, R. K.; Aksay, I. A. *Chem. Mater.* **2007**, *19*, 4396−4404.
(67) Park, S.; An, J.; Piner, R. D.; Jung, I.; Yang, D.; Velamakanni, A.; Nguyen, S. T.; Ruoff, R. S. *Chem. Mater.* **2008**, *20*, 6592−6594.
(68) Park, S.; Ruoff, R. S. *Nat. Nanotechnol.* **2009**, *4*, 217−224.
(69) Stankovich, S.; Dikin, D. A.; Piner, R. D.; Kohlhaas, K. A.; Kleinhammes, A.; Jia, Y.; Wu, Y.; Nguyen, S. T.; Ruoff, R. S. *Carbon* **2007**, *45*, 1558−1565.
(70) Eaton, P.; West, P. *Atomic Force Microscopy*; Oxford University Press: New York, 2010.
(71) Rabe, J. P.; Buchholz, S. *Science* **1991**, *253*, 424−427.
(72) Király, Z.; Findenegg, G. H.; Klumpp, E.; Schlimper, H.; Dekany, I. *Langmuir* **2001**, *17*, 2420−2425.
(73) Quina, F. H.; Nassar, P. M.; Bonilha, J. B. S.; Bales, B. L. *J. Phys. Chem.* **1995**, *99*, 17028−17031.
(74) Thévenot, C.; Grassl, B.; Bastiat, G.; Binana, W. *Colloids Surf., A* **2005**, *252*, 105−111.
(75) Hass, J.; Feng, R.; Millán-Oyoya, J. E.; Li, X.; Sprinkle, M.; First, P. N.; de Heer, W. A.; Conrad, E. H.; Berger, C. *Phys. Rev. B* **2007**, *75*, 214109.
(76) Benrraou, M.; Bales, B. L.; Zana, R. *J. Phys. Chem. B* **2003**, *107*, 13432−13440.
(77) Hayashi, S.; Ikeda, S. *J. Phys. Chem.* **1980**, *84*, 744−751.
(78) Sein, A.; Engberts, J. B. F. N. *Langmuir* **1995**, *11*, 455−465.
(79) Blackburn, J. L.; Barnes, T. M.; Beard, M. C.; Kim, Y.; Tenent, R. C.; McDonald, T. J.; To, B.; Coutts, T. J.; Heben, M. J. *ACS Nano* **2008**, *2*, 1266−1274.
(80) Green, A. A.; Hersam, M. C. *Nano Lett.* **2008**, *8*, 1417−1422.
(81) Miyata, Y.; Yanagi, K.; Maniwa, Y.; Kataura, H. *J. Phys. Chem. C* **2008**, *112*, 3591−3596.
(82) Wanless, E. J.; Ducker, W. A. *Langmuir* **1997**, *13*, 1463−1474.